

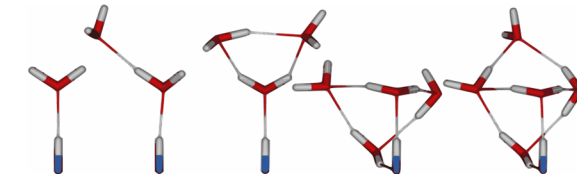
Ground and Excited States Of OH⁻(H₂O)_n Clusters

David Zanuttini* and Benoit Gervais*

CIMAP, ENSICAEN, CNRS, CEA/IRAMIS, Université de Caen, 14070 Caen cedex 05, France

 Supporting Information

ABSTRACT: We present an ab initio study of OH⁻(H₂O)_n ($n = 1-7$) clusters in their lowest three singlet and two triplet electronic states, calculated with the RASPT2 method. Minimum energy structures were obtained by geometry optimization for both (a) the 1¹ Σ^+ ground state and (b) the 1³ Π excited state. From these structures, vertical detachment energies (VDEs), transition energies, and atomic charges were calculated. (a) We found that ground-state geometries present the hydroxide at the surface, accepting three and four H bonds from water. The excess charge is strongly stabilized by water up to a VDE of 6.7 eV for $n = 7$. Bound singlet excited states for ground-state geometries exist for $n \geq 3$, and their VDE increases up to 1 eV for $n = 7$. (b) The 1³ Π state equilibrium geometries completely differ from the ground-state geometries. They are characterized by the hydroxide acting as a single H bond donor to a water molecule, which then donates a H-bond to two others, forming a “tree” pattern. All minimum energy structures present this “tree” pattern and a constant total number of $2n - 2$ H bonds, or equivalently 3 dangling hydrogens. The excess charge stabilizes from $n = 2$ and goes mainly at the surface, on the dangling hydrogens of water. An almost neutral OH radical is then formed. Resulting structural resemblances with the neutral system make the VDEs of the first excited states weakly geometry dependent but size sensitive because of additive polarization effects. In contrast, the 1¹ Σ^+ state at the 1³ Π geometries is strongly sensitive to structural patterns. We bring out existing correlations between these patterns and the corresponding 1¹ Σ^+ state energy increase, which leads to couplings with excited states and possibly to an inversion of the state energy order. From these assessments, we propose a scenario for recombination of aqueous hydroxide following excitation in a charge-transfer-to-solvent state.



Minimum energy structures of OH⁻(H₂O)_{n=1-5} in the 1³ Π excited state.

1. INTRODUCTION

Isolated anions generally do not support excited bound states. Once in a polar solvent, they can exhibit an intense absorption band in the visible UV range. Indeed, solvent polarization influences the stabilization of the excited states, to form quasi-bound intermolecular states, referred to as charge-transfer-to-solvent (CTTS) states. Excitation of the anion in a CTTS state produces a solvated electron, leaving the corresponding neutral species in a more or less close contact pair.¹

The solvation dynamics of the electron, produced by either a CTTS mechanism or water photoexcitation, has received particular experimental attention (see the recent review of Young and Neumark²). The first time-resolved study of the ultrafast generation of hydrated electrons was reported by Miguez et al.³ It provides clear evidence of the existence of a prehydrated state of the electron, which thermalizes in 110 fs and then relaxes in 240 fs toward the fully solvated state. It has been later suggested by Laenen et al.⁴ that this prehydrated electron may be interpreted as a transient state of the electron in some preexisting trapping sites, with a smaller number of involved water molecules than for the fully solvated electron.

The fully solvated electron, which is the simplest hydrated electronic system, was also investigated by different theoretical works.⁵⁻⁸ A practical reason for this attention arises from the ability to model the system as a one-electron system as a first approximation, which enables fast calculations and a straightforward analysis of the excited states. Despite the numerous insights

brought by such studies (for an overview, see the recent review of Turi and Rossky⁹), substantial debates still exist regarding the interior/surface solvation structures of the solvated electron¹⁰ and their relative importance with respect to the size and temperature of the system. Thus, the full microscopic description of the electron solvation and the corresponding dynamics is still a challenge.

Concerning the nature of CTTS states, several theoretical attempts¹¹⁻¹³ have been made to understand the photo-excitation of halide ions in aqueous solutions. In particular, the work of Sheu and Rossky¹⁴ is, to our knowledge, pioneering in the full description of this dynamic process within a one-electron framework, from the halide ion photoexcitation to the recombination. They show that the separation of the halogen:e⁻ pair is prior to any other relaxation channel and that the following indirect-recombination process only occurs once the hydrated electron has relaxed to the s-like lowest CTTS state of a solvent cavity. No direct-recombination process was found, in agreement with experimental measurements.^{15,16} This assessment is in marked contrast with the observed fast geminate recombination process occurring in aqueous hydroxide solutions. It has been suggested that this fast geminate recombination is “uniquely connected to the properties of the hydroxide anion”¹⁶ and that

Received: April 23, 2015

Revised: June 19, 2015

Published: June 19, 2015

new theoretical investigations are required to understand this process at the microscopic level and the enhanced reactivity of the presolvated electron and hydroxyl radical.

These two highly reactive radical species, initiated by either CCTS excitation of aqueous hydroxide or water photoexcitation, present a particular interest.¹⁷ First, regarding safety in nuclear power plants and waste treatment and storage, such species can produce undesirable secondary species, such as explosive dihydrogen, and a premature deterioration of materials all along the nuclear fuel cycle. Second, in the field of radiobiology and radiotherapy, OH radicals and solvated electrons are known to produce oxidative and reductive DNA damage, respectively. Recently, Nguyen et al.¹⁸ reported that the subpicosecond-lived “hot” OH radical and presolvated electron play a more significant role in DNA damage than the corresponding equilibrated “cold” OH and solvated electron. Thus, dynamic features on the formation of these primary species at the subpicosecond time scale are necessary to understand the exact nature of the “hot” OH and the presolvated electron and also the reason these short-lived species display such enhanced reactivities. Their high reactivities support the fast and efficient geminate recombination of the OH[·]e[−] pair, reported in recent femtosecond spectroscopy experiments on aqueous hydroxide following excitation in a CTTS state.^{1,16} In spite of all these experimental efforts, the separation of the pair and whether solvent molecules separate the pair are still undetermined. We may expect that complementary theoretical investigations, and in particular molecular dynamics, would be able to provide new insights into the CTTS state, from its generation via photoexcitation to the recombination or the separation of the pair.

Up to now, almost all of the ab initio studies on OH[−] in water have been based on density functional theory (DFT),¹⁹ Møller–Plesset perturbation theory to second order (MP2),²⁰ or a multistate empirical valence bond model.²¹ These methods are successful in describing the solvation ground state of hydroxide in both water clusters^{22–24} and solution,^{25,26} and the corresponding molecular dynamics in solution reveal that the transport mechanism involves the interplay of specific hydration complexes. However, all of these methods are only suited for the ground state and cannot describe the excited CTTS states or the recombination.

We report in this work a prospective ab initio study of OH[−](H₂O)_n (*n* = 1–7) clusters, relaxed in both the 1¹Σ⁺ ground state and the 1³Π first excited state, performed with restricted active space second-order perturbation (RASPT2) theory. From these structures, we systematically calculate atomic charges, vertical detachment energies (VDEs), and transition energies. From these properties, we intend to understand how the system stabilizes the excess electron and how molecular arrangement influences the transition energy, as a starting point for a further model. An underlying expectation is to identify whether particular structures lead to an energetic inversion of the ground and excited states, the sign of an avoided crossing and a possible pathway for recombination.

We mention that the notation OH[−](H₂O)_{*n*} may be abusive for excited states and should be generalized by the [OH(H₂O)_{*n*}][−] notation, as the excess electron can localize over water molecules rather than OH. However, for the sake of simplicity, we keep throughout this paper the notation OH[−](H₂O)_{*n*}, usually used in the literature.

2. THEORETICAL METHODS

The goal of this ab initio study is to obtain equilibrium geometries and their corresponding VDEs and transition energies.

As it requires dealing with ground and excited states of different chemical natures, nearly degenerate states, and a free radical for the neutral system, only configuration interaction methods can provide a good chemical description and a sufficient accuracy. However, a compromise between computational accuracy and cost is mandatory, as accuracy necessarily demands large basis sets and large configuration spaces, while the optimization process, involving numerous energy gradient evaluations, demands low costs. To fulfill these criteria, we can only act on the reduction of the configuration space and the level of approximation used for the correlation treatment. This can be done with the RASPT2 method.^{27–30} The basic idea of this method is to start with the restricted active space self-consistent field (RASSCF) method,^{27,31} to properly describe the main chemical characteristics of the different electronic states with a few configurations. Then, from each of these reference configurations, we construct single and double excitations and perform an interaction configuration to recover dynamic correlation. This step can be treated either variationally or perturbatively, which leads to the multireference singly and doubly excited configuration interaction (MRSDCI)³² or RASPT2 methods, respectively. The MRSDCI method benefits from variational principle and gives accurate results but suffers from high computational cost. The RASPT2 method is much cheaper but only remains accurate if the perturbation is small enough: i.e., if a proper active space has been selected first.

We select two different active spaces for the RASPT2 method, shared by both ground and excited states: a small space for a fast optimization process and a larger space to calculate molecular properties more accurately.

The minimum active space must describe the main configuration of each desired state of OH[−]. These configurations are composed of a set of three common doubly occupied orbitals {1σ, 2σ, 3σ} and a set of partially occupied orbitals {1π, 1π', 4σ} having the occupation numbers {2, 2, 0} in the 1¹Σ⁺ ground state, {2, 1, 1} in the 1¹Π and 1³Π states, and {1, 2, 1} in the 1¹Π' and 1³Π' states. Note that 1Π and 1Π' molecular states of OH[−](H₂O)_{*n*} correspond to the 1Π_x and 1Π_y states of the free OH[−], respectively. As a water environment mixes the 1Π_x and 1Π_y states and lifts their degeneracy, the *xy* notation no longer holds. Instead, we choose the notation 1Π and 1Π' to refer to the lower and upper states in energy, respectively. The states defined above describe the electronic states of OH[−] only. As water molecules have excitation energies higher than those considered in this work, which spread below 6 eV, the water molecules remain in their 1¹A₁ ground states in all cases.

The partially occupied set {1π, 1π', 4σ} of OH[−] thus forms the minimum active space, composed of a few configurations, that we choose for the optimization process. Our minimum active space possibly shows a significant improvement of the energy over the single-reference MP2 method. Moreover, it does not suffer from spin contamination that exists for open shells in the MP2 method and provides a proper treatment of nearly degenerated states.

In this study, we performed geometry optimization for the 1¹Σ⁺ ground state and for the 1³Π first excited state, which is the ground state of its spin symmetry. The 1³Π state resembles the first excited 1¹Π state optically accessible from the ground state, as their main configuration has the same occupation number of the orbitals. Calculating the 1³Π state is simpler than calculating the 1¹Π state, as it does not have to be orthogonalized with the ground state. Furthermore, if the PES of the 1¹Σ⁺ and 1¹Π states get close enough to each other, the corresponding adiabatic states can strongly mix the main configuration of these

two states, which makes geometry optimization rather tricky. This is not the case for the $1^3\Pi$ state, which does not couple to the singlet states, as we neglect spin–orbit interaction in our Hamiltonian.

Minimum energy structures of $\text{OH}^-(\text{H}_2\text{O})_n$ clusters were obtained by full geometry optimization of several initial arrangements, for each cluster size n . The energy gradient was obtained by numerical differentiation at the RASPT2 level. As an exhaustive study of all isomers, i.e. local minima, is out of reach for a few water molecules, we select a limited set of initial arrangements according to (i) the coordination number, i.e. mainly the hydrogen bond network, (ii) the energy of previously relaxed smaller clusters, and (iii) previous studies for the ground state^{22–24,33} to obtain the lowest energy isomers (LEI). This method ensures a good compromise between a low computational cost and an efficient exploration of the lowest part of the potential energy surface (PES).

Once equilibrium geometries have been obtained, we evaluate the following molecular properties: (i) the energy difference ΔE between an isomer (local minimum) and the lowest energy isomer (LEI) (global minimum), (ii) the mean $\text{OH}^-/\text{H}_2\text{O}$ binding energy, (iii) the vertical detachment energy (VDE), which corresponds to the minimum energy to remove an electron, defined as minus the difference between an isomer energy and its corresponding neutral species energy originating from the $1^2\Pi$ ground state of OH, at the same geometry, (iv) the transition energy between the five lowest electronic states—the $1^1\Sigma^+$ ground state and the $1^1\Pi$, $1^1\Pi'$, $1^3\Pi$ and $1^3\Pi'$ first excited states—and finally (v) the charge carried by each atom.

For molecular properties, we need to compute several electronic states in a single calculation, in order to preserve orthogonality between states and to obtain proper relative energies. RASSCF molecular orbitals are thus state-averaged orbitals: i.e., optimized to lower the energy of all these states simultaneously. However, a given state, for a given active space, is better described within a single-state calculation than within a multistate one. In order to obtain wave functions for molecular properties with at least the same quality as that for geometry optimization, we need to increase the minimum active space with virtual orbitals to recover flexibility in the molecular basis. As these static calculations do not involve numerous energy evaluations for the gradient, we further increased the active space, to lessen the perturbation and to obtain a better convergence of the results. To benchmark the RASPT2 convergence, we select an active space composed of the three partially occupied 1π , $1\pi'$, and 4σ orbitals and n_v lowest virtual orbitals, with at most two electrons in the virtual orbitals. We tested different values of n_v on small clusters, up to two water molecules, to retain a value of seven virtual orbitals, which shows a good compromise between the cost and convergence of the RASPT2 results.

By comparison, variational MRSDCI theory needs only the configuration built on two virtual orbitals, namely the 2π and $2\pi'$ orbitals, to get the same convergence. The difference in n_v values between the two methods means that the configurations that partially occupy the five supplementary virtual orbitals contribute significantly to the wave function and therefore cannot be treated perturbatively. Thus, by adding five virtual orbitals in the active space during the RASSCF calculation, these significant configurations are treated variationally, making it possible to reach a satisfactory accuracy.

Concerning the basis set, the anionic nature of $\text{OH}^-(\text{H}_2\text{O})_n$ requires including both polarization functions, to reproduce the electronic response of water in the field of OH^- , and diffuse

functions, to describe the spread of the weakly bound excited states of OH^- . We thus choose the well-suited aug-cc-pVNZ basis set, introduced by Dunning and co-workers.^{34,35} To make the relaxation step computationally feasible, we limited calculations to valence double- ζ . For property evaluation, triple- ζ and even quadruple- ζ for small clusters were used.

No estimation of the basis set superposition error was made. Indeed, covalent bonding exists inside molecules and through the hydrogen bond network, along with significant charge transfers. Thus, the necessary isolation of atomic or molecular fragments, as in the counterpoise correction,³⁶ becomes artificial, since it does not reproduce the charge state of the fragments and the modification of their orbitals in the total system.^{37,38}

To evaluate the electric charges carried by each atom, we choose the LoProp approach.³⁹ The LoProp scheme shows convergence with the increase of the basis set, in contrast to the widespread Mulliken⁴⁰ or Löwdin⁴¹ population analysis. Furthermore, the straightforward partitioning of the basis functions into occupied and virtual orbitals enables a comparison of the different electronic states and thus a study of the charge transfer process. This is not the case for the popular natural atomic orbital analysis,⁴² because the partitioning relies on the electronic configuration, which differs between different states.³⁹

All ab initio calculations presented throughout this paper were performed at the RASPT2 level, using MOLCAS quantum chemistry software version 7.8,⁴³ and molecular visualizations were done with Molden software.⁴⁴

3. 1 $^1\Sigma^+$ GROUND STATE RELAXED STRUCTURES

3.1. Minimum Energy Structures. Figure 1 gathers the minimum energy structures of $\text{OH}^-(\text{H}_2\text{O})_n$ clusters in their ground state, sorted by size and energy. Table 1 reports the energy difference ΔE between an isomer and the lowest energy isomer, as well as the results of previous studies.^{22–24,33} We mention the remarkable agreement of our results with the lowest energy isomers of $\text{OH}^-(\text{H}_2\text{O})_n$ ($n = 1–6$) optimized by Bryantsev et al. at the B3LYP/6-311++G(2d,2p) level of theory,²³ with some small deviations concerning the bond lengths and angles between OH^- and water molecules.

To understand how water molecules cluster around OH^- , we first focus on the $\text{OH}^-/\text{H}_2\text{O}$ bond, by analyzing in detail the **1a** isomer of $\text{OH}^-(\text{H}_2\text{O})_1$. At a large distance, this bond is purely electrostatic. The leading ion–dipole interaction tends to align the dipole of the water molecule with the negative charge carried by the hydroxide oxygen. However, the **1a** isomer shows a frustrated ion–dipole interaction, as the oxygen of OH^- aligns with one of the no longer symmetric OH bonds of water. This particular alignment reveals a strong reorganization of the electronic cloud of the water molecule along the oxygen–oxygen direction and places the water as a single H-bond donor to OH^- . This H bond is strongly polar, as a significant partial charge transfer of 0.34 e from OH^- to water occurs.

We focus now on the strength variation of this OH^- interaction with water with respect to the number of water molecules in the first coordination shell. To this end, we define the mean $\text{OH}^-/\text{H}_2\text{O}$ binding energy as

$$\tilde{E}(\text{OH}^-/\text{H}_2\text{O}) = -\frac{E_{\text{OH}^-(\text{H}_2\text{O})_n}^{\text{tot}} - E_{\text{OH}^-}^{\text{min}} - E_{(\text{H}_2\text{O})_n}^{\text{min}}}{n_{\text{OH}^-/\text{H}_2\text{O}}} \quad (1)$$

with $E_{\text{OH}^-(\text{H}_2\text{O})_n}^{\text{tot}}$ being the total energy of $\text{OH}^-(\text{H}_2\text{O})_n$ in the ground state, $E_{\text{OH}^-}^{\text{min}}$ being the energy of the free OH^- in the

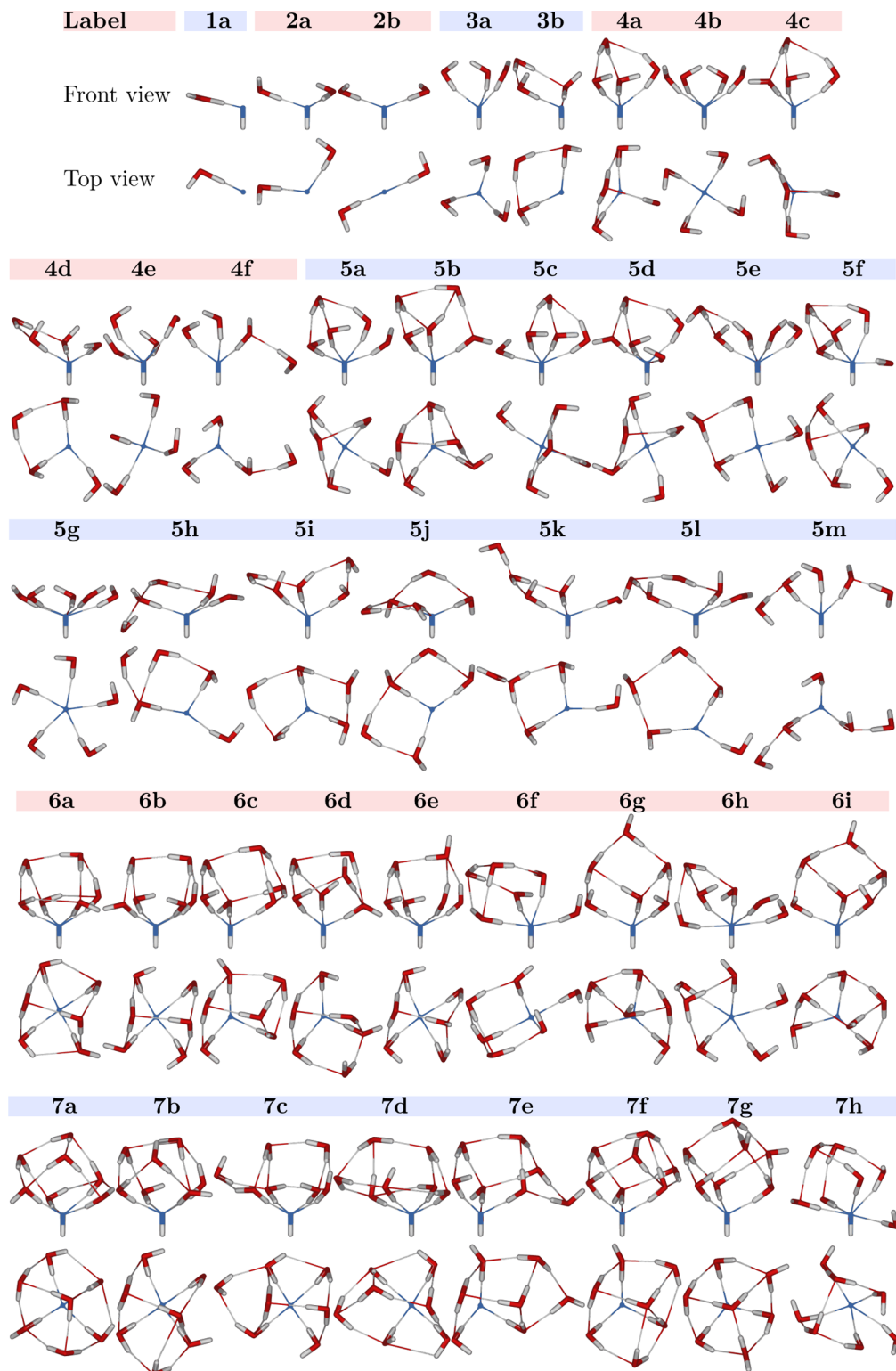


Figure 1. Minimum energy structures of $\text{OH}^-(\text{H}_2\text{O})_n$ (Oxygen O given in blue and water O in red) optimized in the ${}^1\Sigma^+$ ground state, at the RASPT2/aug-cc-pVDZ level. Isomers are sorted by increasing energy; thus, the letters a, b, etc. in isomer labels correspond to the first, second, etc. lowest energy isomers.

ground state at equilibrium geometry, $E_{(\text{H}_2\text{O})_n}^{\min}$ being the energy of the free water clusters $(\text{H}_2\text{O})_n$ in the ground state at equilibrium geometry, and $n_{\text{OH}^-/\text{H}_2\text{O}}$ being the number of water molecules in the first solvation shell or equivalently the number of $\text{OH}^-/\text{H}_2\text{O}$ bonds. Water clusters were taken from the Cambridge database⁴⁵ and then relaxed with the aforementioned RASPT2 method. The results are shown in Figure 2.

The lowest energy isomers **1a**, **2a**, **3a**, **4b**, and **5g** (solid black line), for which all water molecules are bound to the hydroxide, e.g. $n_{\text{OH}^-/\text{H}_2\text{O}} = n$, represent the simplest isomers to analyze the $\text{OH}^-/\text{H}_2\text{O}$ binding energy, as all water molecules are equivalent and weakly interacting. As $n_{\text{OH}^-/\text{H}_2\text{O}}$ increases from 1 to 5, the mean binding energy of the $\text{OH}^-/\text{H}_2\text{O}$ bond decreases from 1.22 to 0.48 eV, along with a lengthening of 1 bohr. Indeed, the partial

Table 1. Difference ΔE of the 1^{Σ}^+ State Energy between an Isomer and the Lowest Energy Isomer (LEI)^a

isomer	ΔE (kcal/mol)						
	this work			ref 22	ref 33	ref 23	ref 24
	VDZ	VTZ	VQZ				
1a	LEI	LEI	LEI	LEI	LEI	LEI	
2a	LEI	LEI	LEI				
2b	0.31	0.24	0.19	LEI	LEI	LEI	
3a	LEI	LEI	LEI	LEI	LEI	LEI	
3b	1.00	0.62	0.69	2.40	1.38		
4a	LEI	LEI	LEI		LEI	LEI	
4b	-0.15	0.21	0.36	1.89	LEI	0.05	0.30
4c	0.49	0.45	0.41	2.70			0.62
4d	1.32	1.26	1.13		0.21		
4e	2.14	2.10	2.13	LEI			0.69
4f	4.63	4.84	4.79	1.11	4.84		
5a	LEI	LEI				LEI	
5b	0.89	0.65					
5c	1.78	1.75			LEI		
5d	2.78	2.60					
5e	2.73	2.78			1.98		
5f	3.12	2.92					
5g	3.76	3.67			1.78		
5h	4.28	3.90					
5i	4.40	3.96		0.99			
5j	5.25	4.79		0.51			
5k	5.54	5.19		LEI			
5l	6.24	5.85		0.90			
5m	8.60	8.60		1.29			
6a	LEI	LEI				LEI	
6b	0.35	0.43					
6c	1.92	1.57					
6d	2.14	1.84					
6e	2.57	2.56					
6f	3.93	3.70					
6g	4.24	3.97					
6h	4.28	4.12					
6i	4.46	4.27					
7a	LEI	LEI					
7b	1.70	1.60					
7c	2.52	2.51					
7d	3.28	3.29					
7e	3.57	3.31					
7f	3.69	3.32					
7g	4.37	4.38					
7h	4.48	4.77					

^aEnergies are calculated at the RASPT2/aug-cc-pVNZ level, where N = D, T, Q, at geometries optimized in the 1^{Σ}^+ ground state (cf. Figure 1). The results of previous works are reported at the DFT(B3LYP)/6-31+G*,²² MP4/aug-cc-pVDZ,³³ MP2/CBS +ΔCCSD(T),²³ and MP2/6-31+G*²⁴ levels.

charge transfer from OH^- to water is almost constant whatever the value of n and saturates to about 0.4 e. While in the 1a isomer the partial charge is carried by a single water molecule, for $n \geq 2$ it is shared by several molecules, making the $\text{OH}^-/\text{H}_2\text{O}$ bond strength lessen as n increases. The effect of adding water molecules in the second solvation shell is visible in Figure 2 following points of a given color, e.g. for a given $n_{\text{OH}^-/\text{H}_2\text{O}}$, as n increases. This effect is to strengthen the $\text{OH}^-/\text{H}_2\text{O}$ bonds and reflects the polarization of the water molecules in the second solvation shell by the hydroxide, screened by the first shell.

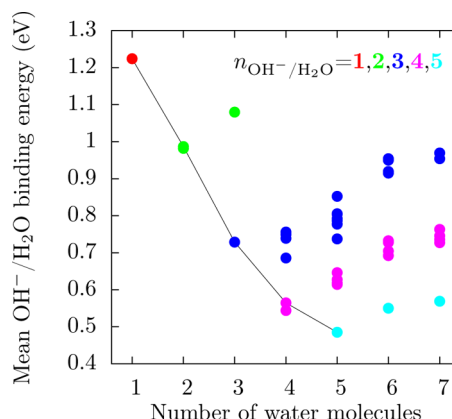


Figure 2. Mean $\text{OH}^-/\text{H}_2\text{O}$ binding energy for $\text{OH}^-(\text{H}_2\text{O})_n$ clusters, defined by eq 1, with respect to the number of water molecules and to the number of $\text{OH}^-/\text{H}_2\text{O}$ bonds. The results are calculated at the RASPT2/aug-cc-pVTZ level, at geometries optimized in the 1^{Σ}^+ ground state (cf. Figure 1). The solid black line corresponds to the lowest energy isomers for which all water molecules are bound to the hydroxide. A given color corresponds to a given number of $\text{OH}^-/\text{H}_2\text{O}$ bonds, whatever the cluster size n .

From five $\text{OH}^-/\text{H}_2\text{O}$ bonds, steric effects arise, in addition to the growing repulsion between the water hydrogens bound to OH^- . As a result, a structure with five $\text{OH}^-/\text{H}_2\text{O}$ bonds becomes energetically unfavorable and a structure with six such bonds is even unstable.

As the leading $\text{OH}^-/\text{H}_2\text{O}$ interaction weakens as $n_{\text{OH}^-/\text{H}_2\text{O}}$ increases, a competition starts between adding a water molecule either in the first or in the second solvation shell of OH^- . In contrast to a water molecule in the first solvation shell, one in the second shell is free to move and to optimize its bonding with other water molecules. It can therefore create two or three true—not frustrated— $\text{H}_2\text{O}/\text{H}_2\text{O}$ bonds, without modifying significantly the inclination of preexisting water molecules of the first solvation shell, as we can see on the 3b and 4a isomers in comparison to 2a and 3a, respectively.

Up to $n = 3$, water molecules bind directly to the hydroxide. From $n = 4$, all the lowest energy isomers show a three or four $\text{OH}^-/\text{H}_2\text{O}$ bond pattern. From this three- and four-bond patterns, additional water molecules in the second solvation shell organize themselves to maximize the coordination number of the hydrogen bond network and lower the total energy. Fine differentiation of isomers having the same coordination number is governed by a subtle orientation of the less bound water molecules, which favors the compactness of the structures. This phenomenon accounts for the 18 and 14 meV energy differences between the 4a and 4c isomers and between the 5d and 5f isomers, respectively.

From $n = 5$, the most stable structure is systematically based upon a four-bond, rather than a three-bond, pattern. This trend does not originate from the $\text{OH}^-/\text{H}_2\text{O}$ interaction but from the intrinsic properties of water clusters, which favor cuboid geometries. Indeed, Maheshwary and co-workers⁴⁶ showed that $(\text{H}_2\text{O})_{4n}$ clusters, of tetrameric ring-based structures, present an enhanced stability, in comparison to the equivalent trimeric $(\text{H}_2\text{O})_{3n}$ or pentameric $(\text{H}_2\text{O})_{5n}$ ring-based clusters. The low-energy isomers of $\text{OH}^-(\text{H}_2\text{O})_n$ based upon a three-bond pattern actually have to form an angularly strained trimeric water ring, in order to maximize the coordination number (see 5b, 6c, and 7d isomers for example), while the four-bond pattern clusters do not.

The comparison from this finite size system to the bulk phase is not straightforward, as the possible configurations of water are so many that strained rings can be avoided. Furthermore, the OH^- molecule, which in clusters remains at the surface, is completely solvated in the bulk phase, with a possible formation of a weak $\text{OH}^-/\text{H}_2\text{O}$ bond via the hydroxide hydrogen.^{47,48} This solvation in the bulk phase can change the relative stability of the three- and four-bond patterns. Moreover, in the liquid at 300 K, the dynamics controls the balance between various coordinations of OH^- .

3.2. Vertical Detachment Energies and Transition Energies. The VDEs of the five lowest states of $\text{OH}^-(\text{H}_2\text{O})_n$ clusters, at the geometries optimized in the ground state, are displayed in Figure 3. They are calculated as the energy difference

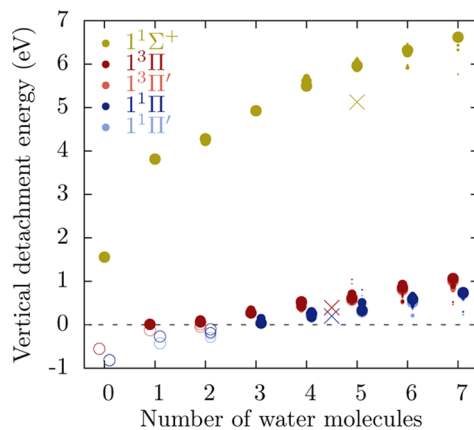


Figure 3. Vertical detachment energies of the five lowest states ($1^1\Sigma^+$, $1^3\Pi$, $1^3\Pi'$, $1^1\Pi$, and $1^1\Pi'$) of $\text{OH}^-(\text{H}_2\text{O})_n$ at geometries optimized in the $1^1\Sigma^+$ ground state (cf. Figure 1). The results are calculated at the RASPT2/aug-cc-pVTZ level. The following symbol legend is common to Figures 4, 6 and 8: filled circle symbols correspond to bound states, while open circle symbols correspond to unbound states (with an energy above the neutral species). The circle area is proportional to the Boltzmann factor $\exp(-k_B T/\Delta E)$ at 300 K to reflect the abundance of the different isomers, with ΔE being the energy difference between the considered isomer and its corresponding lowest energy isomer (cf. Table 1). A cross symbol (X) marks the “solvated” isomer with a water molecule accepting an H-bond from the hydroxide hydrogen atom, as described in the section 3.2.

between one of the five lowest states of $\text{OH}^-(\text{H}_2\text{O})_n$ and the $1^2\Pi$ ground state of the corresponding neutral species $\text{OH}(\text{H}_2\text{O})_n$. While the aug-cc-pVDZ basis set is well-adapted to the neutral species, the ground and excited states of the anionic species demand a larger basis set. The presented results are thus calculated with the aug-cc-pVTZ basis set. This significantly improves the VDEs by +0.2 eV on average, with respect to the aug-cc-pVDZ basis set. In contrast, only very small differences are found with our aug-cc-pVQZ calculations, made for n up to 4.

Concerning the $1^1\Sigma^+$ ground state, for which geometries have been optimized, the presence of water molecules strongly stabilizes the hydroxide. Starting with a value of 3.8 eV for $n = 1$, the VDE grows monotonically with n , to reach 6.6 eV for $n = 7$. This trend is in good agreement with the previous work of Masamura,³³ who performed these calculations at the MP2/aug-cc-pVDZ level. However, these calculations present systematic mean shifts of 0.4 and 0.2 eV above our values with the aug-cc-pVDZ and aug-cc-pVTZ basis sets, respectively. The origin of this discrepancy probably arises from the fact that the MP2

method failed to provide a description of the hydroxyl radical as good as the closed-shell hydroxide.⁴⁹

Several experimental works have described photoelectron emission spectroscopy carried out in aqueous solution and reported a threshold of VDEs in a range from 8.26 eV^{50,51} to 8.45 eV.⁵² Thus, seven water molecules already enable recovery of 75% of the stabilization energy of hydroxide in aqueous solution. The remaining 25% mainly reflects the long-range polarization of water molecules in the third, fourth, etc. solvation shells by the negative charge of OH^- . This polarization is enhanced in solution, as the hydroxide is fully solvated, in contrast to the case for clusters where the hydroxide remains at the surface.

However, in the bulk phase, molecular dynamics⁴⁸ and X-ray diffraction⁵³ studies reveal that water frequently creates a weak H bond with hydroxide via the hydroxide hydrogen. To obtain qualitative effects of this additional water molecule in the first solvation shell of the hydroxide, we study a “solvated” isomer composed of the 4-fold-coordinated isomer **4b** plus a water molecule accepting a 2.10 Å H bond from the hydroxide. In clusters, the position of the latter molecule is not stable. Geometry optimization systematically leads to the migration of the additional water toward the others, breaking the weak H-bond and leaving the hydroxide at the surface. In solution, the pressure of the water environment prevents the migration, and the weak H bond remains stable and spreads in a range from 1.77 to 2.22 Å, as reported from ab initio molecular dynamics simulations⁵⁴ and neutron diffraction experiments.⁴⁷ In order to mimic the first solvation shell in solution, we choose not to relax the “solvated” cluster to preserve this weak H bond. The effect of this weak H bond is depicted by cross symbols in Figures 3 and 4.

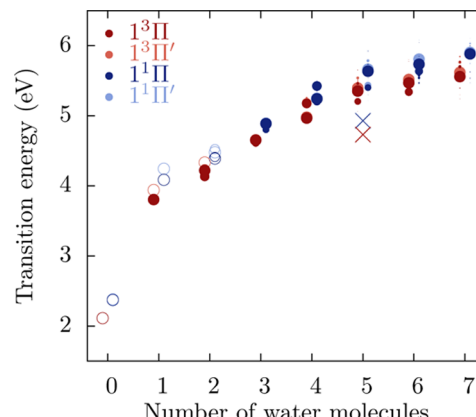


Figure 4. Transition energies from the ground state ($1^1\Sigma^+$) to the four lowest excited states ($1^3\Pi$, $1^3\Pi'$, $1^1\Pi$, $1^1\Pi'$) of $\text{OH}^-(\text{H}_2\text{O})_n$ clusters, at geometries optimized in the $1^1\Sigma^+$ ground state (cf. Figure 1). Results are calculated at the RASPT2/aug-cc-pVTZ level. For the symbol legend, see Figure 3.

It clearly raises the $1^1\Sigma^+$ state energy by about 0.5 eV, while the energies of the $1^1\Pi$, $1^1\Pi'$, $1^3\Pi$, and $1^3\Pi'$ states of the corresponding excited OH^- and that of the $1^2\Pi$ state of the OH are left unchanged. Consequently, the effect of closing the first solvation shell with a water molecule on the hydrogen side of OH, as in an aqueous environment, is to lower the transition energy from the ground state to the excited states.

From the geometries of our $1^1\Sigma^+$ minimum energy structures, vertical transitions can occur either via a dipolar transition toward the singlet states, $1^1\Pi$ and $1^1\Pi'$, or via a less efficient exchange scheme in the case of electron collision toward the triplet states,

$1^3\Pi$ and $1^3\Pi'$. Obviously, such a transition energy is meaningful provided that the excited states are bound: i.e., provided that their VDE is positive. From the excited state VDEs, plotted in Figure 3, we are able to determine how many water molecules are needed for this.

The VDEs of $1^1\Pi$ and $1^3\Pi$ excited states almost linearly increase with n , starting from a negative value for $n = 0$, i.e. unbound states, to reach 0.8 and 1.0 eV for $n = 7$, respectively. Surprisingly, for the triplet $1^3\Pi$ state, a single water is enough to obtain a bound state, while for the $1^3\Pi'$, $1^1\Pi$, and $1^1\Pi'$ states, at least three water molecules are necessary. These differences between states can be explained with the difference between singlet and triplet Π states and the lifting of degeneracy. Indeed, the $1^3\Pi$ states of $\text{OH}^-(\text{H}_2\text{O})_n$ ($n = 1, 2$) are weakly bound, with a typical VDE of 70 meV, whereas the singlet states are approximately 250 meV less bound than their corresponding triplet states, whatever the geometry. Furthermore, the lifting of degeneracy between Π states of the same spin multiplicity is particularly large for one and two water molecules, up to 150 meV, because the first solvation shell naturally breaks the Π symmetry, while for $n \geq 3$, the three- and four-bond coordination patterns of the first solvation shell do not.

Transition energies between the $1^1\Sigma^+$ ground state and the first excited states are plotted in Figure 4 and provide useful information for experimentalists. We emphasize that transition energies, as well as VDEs, are significantly sensitive to the number of water molecules and to a lesser extent to the geometry differences between isomers. The first dipolar transition from $1^1\Sigma^+$ to $1^1\Pi$ states appears at $n = 3$ with a value of 4.9 eV, and increases to reach 5.9 eV at $n = 7$. In comparison, the corresponding energy of the center of the CTTS band in the aqueous phase has been measured by UV spectroscopy techniques,^{55,56} and values around 6.60 eV were reported.

4. $1^3\Pi$ EXCITED STATE RELAXED STRUCTURES

4.1. Minimum Energy Structures. In solution, CTTS states are bound and originate from the excited states of Π symmetry of OH^- . Figure 5 gathers all studied minimum energy structures of $\text{OH}^-(\text{H}_2\text{O})_n$ optimized in the $1^3\Pi$ state up to $n = 7$, sorted by size and energy. The corresponding energy differences ΔE between an isomer and the lowest energy isomer are displayed in Table 2.

For $\text{OH}^-(\text{H}_2\text{O})_1$, we try numerous initial arrangements, presenting either the oxygen or the hydrogens of water to the top, the middle, or the bottom of OH^- , to provide an exhaustive search of minimum energy structures and the underlying principles for the excess electron stabilization, on excitation in the $1^3\Pi$ state. None of them are bound: i.e., the anion energy is above the neutral energy. We notice, however, that the LEI **1a** is made up of an OH acting as an H-bond donor, with the water oxygen centered in a tetrahedral-like structure, in which three of the four vertices are carried by the hydrogens. This configuration reveals a very efficient process to transfer the electron from OH to the water. Indeed, at this geometry, the charge originally located on the O site of OH in the ground state is transferred by 90% toward water, mainly on its dangling hydrogen atoms (dangling Hs).

This configuration still holds when adding water molecules. Indeed, all of the most stable isomers, up to $n = 7$, present a single water molecule as a H-bond acceptor from OH, via the water oxygen. They also present, as isomer **1a** does, a significant charge transfer from OH to the water after excitation from the ground state. Thus, it appears that the water molecule in a H-bond

acceptor position may play a key role in the CTTS process. Isomers differing from this configuration, in particular isomers **1b**, **1d**, **2e**, **3k**, **3l**, **4l**, and **5k**, which favor the localization of the excess charge on the hydroxide hydrogen, systematically display an energy significantly above that of their corresponding LEI. Therefore, they do not exist at room temperature and will no longer be discussed.

Starting from the isomer **1a**, the arrangement of water molecules is as usual governed by the H-bond network: i.e., by maximizing the coordination numbers and by optimizing orientation of the water molecules. However, at the same time, the electron needs the dangling Hs of water to be efficiently stabilized. For a given number of water molecules n , the sum of the H bonds and dangling Hs is constant and simply equals the number of H atoms in the system: i.e., $2n + 1$. Nevertheless, the covalent character of the H bonds makes them directional and prevents the formation of $2n + 1$ of them, because of geometric considerations. The most compact structure enables creation of at most $2n - 1$ H bonds, leaving 2 dangling Hs. However, this compact structure can undergo strong constraints from the tight trimeric H-bond cycle. Therefore, it can be energetically favorable to break one or a few H bonds to open up the structure and lessen the constraints. Furthermore, a H-bond break releases a supplementary H atom, which can help the stabilization of the excess electron.

The number of H bonds alone does not exclusively define the energy. Actually, a specific pattern arises from minimum energy structures. The “tree” pattern, with the first water molecule accepting a H bond from an OH H site and donating a H bond to the second and third water molecules, is displayed by the isomer **3a** or **3b** in Figure 5. It ensures an efficient transfer of the electron from OH toward the dangling Hs of water. The tree pattern still holds for the lowest energy isomers of $\text{OH}^-(\text{H}_2\text{O})_n$ for $n > 3$ and is prior to any other H-bond motif. In contrast, isomers **2b**, **3c**, and **4c** display an extra H bond in comparison to the isomers **2a**, **3b**, and **4b**, respectively, and we would therefore expect the former to be lower in energy. However, as they do not show the tree pattern, their energy is systematically above that of the latter.

The stabilization of the excess electron, following the excitation of OH^- in the $1^3\Pi$ state, is made possible by the presence of dangling Hs and to a lesser extent by the H-bond network. The stabilization effect arising from the H-bond network is directly linked to the cluster size. This effect is visible by comparing the isomers **1a** and **2b**, for example, in Figure 5. Each of them displays two dangling Hs. However, the **1a** isomer does not bind the $1^3\Pi$ state while the **2b** isomer does. This weak effect is mandatory, as none of the $\text{OH}^-(\text{H}_2\text{O})_n$ clusters bind the $1^3\Pi$ state, while all of the $\text{OH}^-(\text{H}_2\text{O})_n$ clusters with $n \geq 2$ do, whatever their number of dangling Hs. The H-bond network thus defines a minimum size, $n = 2$, that enables the stabilization of the $1^3\Pi$ state.

Concerning the dangling Hs, two of them are enough to bind the excess charge. For the corresponding **2b** and **4h** isomers, the two dangling Hs belong to a single water molecule and carry around 75% of the charge, while the oxygen site of the same molecule carries 10%. The remaining 15% of the charge is equally distributed over the neighboring atoms of water and hydroxyl molecules. Though two dangling Hs are enough to bind the excess electron, we found that all the lowest energy isomers have three of them. The reason for this is not only a better stabilization of the electron when the number of dangling Hs is increased but also, as we have seen previously in this section, the existing

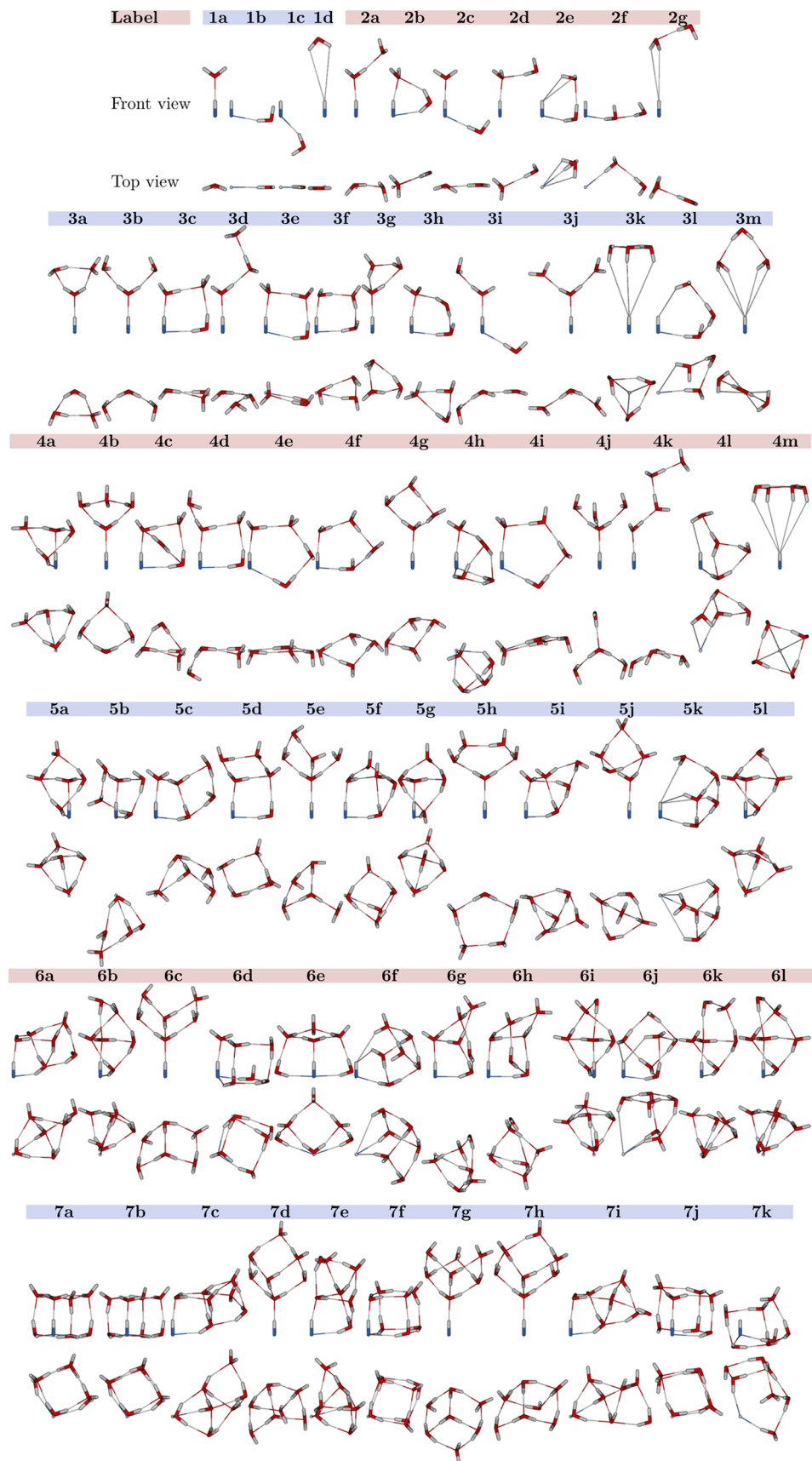


Figure 5. Minimum energy structures of $\text{OH}^-(\text{H}_2\text{O})_n$ (Oxygen O given in blue and water O in red) optimized in the $1^3\Pi$ excited state, at the RASPT2/aug-cc-pVDZ level. Isomers are sorted by increasing energy; thus, the letters a, b, etc. in isomer labels correspond to the first, second, etc. lowest energy isomers.

Table 2. Difference ΔE of the $1^3\Pi$ State Energy between an Isomer and the Lowest Energy Isomer (LEI)^a

Isomer	ΔE (kcal/mol)			Isomer type OH donor Tree(●)/Chain(●) OH acceptor “AA” motif OH non-acceptor .(tree/chain)	Isomer	ΔE (kcal/mol)			Isomer type OH donor Tree(●)/Chain(●) OH acceptor “AA” motif OH non-acceptor .(tree/chain)
	VDZ	VTZ	VQZ			VDZ	VTZ		
1a	LEI	LEI	LEI	● ○ ○ ○ ○	4m	6.56	4.78	○ ○ ○ ○ ○	
1b	4.36	3.51	3.33	○ ○ ● ○ ○	5a	LEI	LEI	● ○ ○ ○ ○	
1c	6.58	5.48	5.01	○ ○ ● ○ ○	5b	0.80	0.71	● ○ ○ ○ ○	
1d	4.80	6.14	6.52	○ ○ ○ ○ ○	5c	1.37	1.75	● ○ ○ ○ ○	
2a	LEI	LEI	LEI	● ○ ○ ○ ○	5d	1.72	1.95	● ○ ○ ○ ○	
2b	1.18	1.18	1.24	● ○ ○ ○ ○	5e	2.46	2.48	● ○ ○ ○ ○	
2c	2.02	1.90	1.87	● ○ ○ ○ ○	5f	2.91	2.65	● ○ ○ ○ ○	
2d	1.32	1.94	2.09	● ○ ○ ○ ○	5g	3.73	3.38	● ○ ○ ○ ○	
2e	4.54	3.40	4.18	○ ○ ○ ○ ○	5h	3.34	3.67	● ○ ○ ○ ○	
2f	4.96	4.12	4.35	○ ○ ○ ○ ○	5i	4.10	3.68	● ○ ○ ○ ○	
2g	5.42	4.22	4.54	○ ○ ○ ○ ○	5j	3.64	4.32	● ○ ○ ○ ○	
3a	LEI	LEI	LEI	● ○ ○ ○ ○	5k	5.26	4.50	○ ○ ○ ○ ○	
3b	-0.27	0.03	0.21	● ○ ○ ○ ○	5l	5.44	4.66	● ○ ○ ○ ○	
3c	-0.28	0.06	0.19	● ○ ○ ○ ○	6a	LEI	LEI	● ○ ○ ○ ○	
3d	0.35	0.17	0.04	● ○ ○ ○ ○	6b	0.01	0.08	● ○ ○ ○ ○	
3e	0.11	0.34	0.56	● ○ ○ ○ ○	6c	-0.72	0.54	● ○ ○ ○ ○	
3f	0.71	0.47	0.43	● ○ ○ ○ ○	6d	0.16	1.12	● ○ ○ ○ ○	
3g	1.61	1.44	1.39	● ○ ○ ○ ○	6e	1.50	2.62	● ○ ○ ○ ○	
3h	1.51	1.90	1.96	● ○ ○ ○ ○	6f	2.59	2.81	○ ○ ○ ○ ○	
3i	2.63	2.36	2.35	● ○ ○ ○ ○	6g	2.31	3.33	● ○ ○ ○ ○	
3j	4.46	3.93	4.02	● ○ ○ ○ ○	6h	2.36	3.63	● ○ ○ ○ ○	
3k	5.92	4.22	4.47	○ ○ ○ ○ ○	6i	2.98	3.76	● ○ ○ ○ ○	
3l	5.48	4.80	5.01	○ ○ ○ ○ ○	6j	3.80	4.03	○ ○ ○ ○ ○	
3m	7.33	5.76	6.03	○ ○ ○ ○ ○	6k	3.73	5.00	● ○ ○ ○ ○	
4a	LEI	LEI	-	● ○ ○ ○ ○	6l	4.95	5.01	● ○ ○ ○ ○	
4b	-0.52	0.06	-	● ○ ○ ○ ○	7a	LEI	LEI	● ○ ○ ○ ○	
4c	1.52	1.80	-	● ○ ○ ○ ○	7b	-0.18	0.02	● ○ ○ ○ ○	
4d	1.97	2.31	-	● ○ ○ ○ ○	7c	-0.02	0.42	● ○ ○ ○ ○	
4e	2.11	2.43	-	● ○ ○ ○ ○	7d	-1.01	0.54	● ○ ○ ○ ○	
4f	2.90	2.59	-	● ○ ○ ○ ○	7e	0.40	0.62	● ○ ○ ○ ○	
4g	2.63	2.59	-	● ○ ○ ○ ○	7f	1.77	1.72	● ○ ○ ○ ○	
4h	3.12	2.68	-	● ○ ○ ○ ○	7g	0.44	1.80	● ○ ○ ○ ○	
4i	3.21	3.52	-	● ○ ○ ○ ○	7h	3.31	3.75	● ○ ○ ○ ○	
4j	3.09	3.52	-	● ○ ○ ○ ○	7i	4.08	3.94	● ○ ○ ○ ○	
4k	3.46	3.52	-	● ○ ○ ○ ○	7j	3.48	4.34	● ○ ○ ○ ○	
4l	5.37	4.41	-	○ ○ ○ ○ ○	7k	5.95	5.45	○ ○ ○ ○ ○	

^aEnergies are calculated at the RASPT2/aug-cc-pVNZ level, where N = D, T, Q, at geometries optimized in the $1^3\Pi$ excited state (cf. Figure 5). Color-filled circles display the main features of isomers, and their meaning is common with that in Figures 7 and 9: (dark blue, OH donor) hydroxyl hydrogen gives a H bond to a water molecule; (light blue, Tree) tree pattern, described in section 4.1, present; (gray-green, Chain) chain pattern, as displayed by isomers 2a, 3d and 4k of Figure 5, present; (red, OH acceptor) hydroxyl oxygen accepts a H bond from a water molecule; (orange-yellow, “AA” motif) “AA” motif, i.e. two dangling Hs from the same water molecule, present; (purple, OH non-acceptor-(tree+chain)) hydroxyl oxygen does not accept a H bond from a water molecule but tree pattern or chain pattern present.

strong constraints in the most compact structures containing only two dangling Hs. The latter contains a tight, i.e. energetically unfavorable, trimeric ring, as in the isomers 2b and 4h. Such structures are not stable for $n = 3, 5$, and their relaxation leads to a H-bond break in the trimeric ring, thus opening the structures.

Now, consider structures with more than three dangling Hs. The loss of the corresponding H bonds is not compensated by a better stabilization of the excess electron. Indeed, atomic charges calculated with the LoProp method reveals that the excess electron is typically localized on two or three dangling Hs and that a fourth, fifth, etc. dangling H does not participate in the charge stabilization. This statement has been previously pointed out by Herbert and Head-Gordon, in their theoretical study of small $(\text{H}_2\text{O})_n^-$ clusters,⁵⁷ on the basis of natural population analysis for relaxed structures.

Another similarity with $(\text{H}_2\text{O})_n^-$ clusters is the enhanced stability of the excess electron bound by the dangling Hs, when two of the latter belong to the same water molecule, rather than to different molecules. Indeed, this double H-bond acceptor, or “AA” motif, has been revealed as a dominant feature for anionic water clusters up to eight water molecules, by infrared spectroscopy measurements coupled with ab initio studies.^{57–59} In the case of $\text{OH}^-(\text{H}_2\text{O})_n$ clusters, all of the lowest isomers present the “AA” motif, except for $n = 6, 7$, which only display single H-bond acceptor motifs. The case of $\text{OH}^-(\text{H}_2\text{O})_6$ and $\text{OH}^-(\text{H}_2\text{O})_7$ clusters is actually particular. Due to limited water acceptance and geometric considerations, the “AA” motif cannot be formed without compromising previous clustering patterns: i.e., the tree pattern and the maximum number $2n - 2$ of H bonds. This trend appears more clearly for cuboid clusters, such as the 7a, 7b, and 7j isomers. In these isomers, water molecules

are placed at the vertices of the cube, so that each of them forms three H-bonds. To free the two hydrogen atoms of a single water molecule, the latter has thus to be a triple acceptor such as the 7j isomer, which is energetically unfavorable. In the same spirit, both 6a and 6h isomers display the tree pattern. The former forms $2n - 2$ H bonds and no "AA" motif, while the latter has one H bond less to provide the "AA" motif, which increases its energy by 150 meV. Therefore, the "AA" motif is a weaker requirement in comparison to formation of the maximum number of H bonds.

From these results, we found the systematic clustering requirements common to all the minimum energy structures of $\text{OH}^-(\text{H}_2\text{O})_n$ in the $1^3\Pi$ state, in descending order of importance by forming:

1. the tree pattern
2. the maximum number $2n - 2$ of unconstrained H bonds, or equivalently 3 dangling hydrogen atoms
3. the "AA" motif, if possible

4.2. Vertical Detachment Energies. Figure 6 displays vertical detachment energies (VDEs) for the three lowest singlet

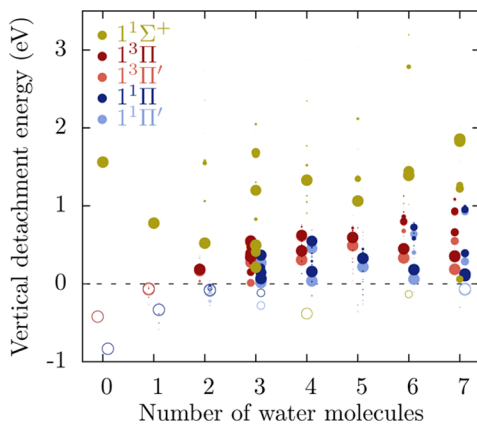


Figure 6. Vertical detachment energies of the five lowest states ($1^1\Sigma^+$, $1^3\Pi$, $1^3\Pi'$, $1^1\Pi$, and $1^1\Pi'$) of $\text{OH}^-(\text{H}_2\text{O})_n$ clusters, at geometries optimized in the $1^3\Pi$ first excited state (cf. Figure 5). The results are calculated at the RASPT2/aug-cc-pVTZ level. For the symbol legend, see Figure 3.

states ($1^1\Sigma^+$, $1^1\Pi$, and $1^1\Pi'$) and the two lowest triplet states ($1^3\Pi$ and $1^3\Pi'$), at the equilibrium geometry of the $1^3\Pi$ state.

Regarding first the VDEs of the $1^1\Sigma^+$ state, we notice a remarkably smaller binding, in comparison to geometries optimized in the $1^1\Sigma^+$ state (cf. Figure 3). The main reasons for this phenomenon are 2-fold. First, the enhanced stabilization of the $1^1\Sigma^+$ state occurs when several water molecules give a H bond to the hydroxyl oxygen atom, as we have seen for $1^1\Sigma^+$ structures (cf. Figure 1). This is no longer the case for $1^3\Pi$ optimized structures (cf. Figure 5), which display none, one, or rarely two such bonds. Second, the most stable geometries relaxed in the $1^3\Pi$ state give rise to a strong charge transfer to the dangling Hs of water. As a result, the bonding network is very similar to that of the neutral $\text{OH}(\text{H}_2\text{O})_n$ clusters, perturbed by the excess electron. Consequently, the optimization of structures in the $1^3\Pi$ state also optimizes, to a smaller extent, the $1^2\Pi$ state of neutral clusters. The VDEs for the $1^1\Sigma^+$ state between different isomers present an important spreading, in a range up to 2 eV, among a given size n . We shall go back to this point in detail later in section 4.3, for the study of transition energies, but it is intimately linked to the closest environment of OH.

Concerning the VDEs of Π states, they essentially follow the same trend as for $1^1\Sigma^+$ structures, even though the two sets of geometries display very different structural features. Figure 7 displays detailed information on their distribution. Black hollow circles represent the VDEs of the $1^3\Pi$ state for $1^3\Pi$ structures given in Figure 7a and are repeated in all panels. A comparison with the $1^1\Sigma^+$ structures, represented with yellow-filled circles, is given in Figure 7b. With the exception of the broader distribution for $1^3\Pi$ structures, mean values are very similar. The relative constant VDEs of the $1^3\Pi$ state, whatever the geometry, reflects the close chemical nature between Π states of anionic clusters and the $1^2\Pi$ state of neutral clusters. All of these states actually show similar clustering patterns, except for the stabilization of the excess electron. As a result, their corresponding PESs are almost parallel and vary in a similar manner for a given atomic displacement.

However, the presence of the excess electron for anionic Π states induces significant water polarization, which does not exist for the neutral species. This polarization grows with the number of water molecules and is responsible for the almost linear increase of VDEs of Π states. As for the $1^1\Sigma^+$ state, we also notice

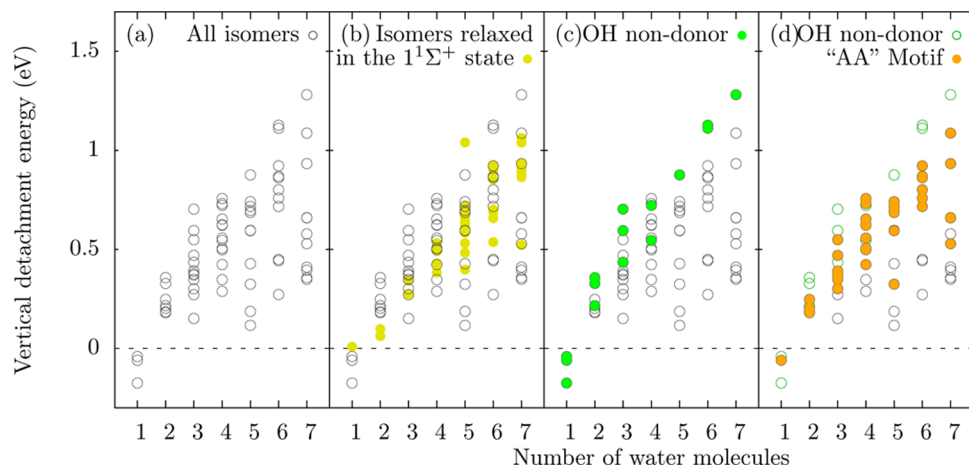


Figure 7. Vertical detachment energies (VDEs) of the $1^3\Pi$ state of $\text{OH}^-(\text{H}_2\text{O})_n$ clusters, at geometries optimized in the $1^3\Pi$ first excited state (cf. Figure 5). The results are calculated at the RASPT2/aug-cc-pVTZ level. Black open circles in all panels display all isomers, and solid circles in panels c and d display the isomers fulfilling the selected criterion: (a) all isomers (\circ); (b) VDEs of the $1^3\Pi$ state, at geometries optimized in the $1^1\Sigma^+$ state (yellow-green \bullet) (cf. Figure 1); (c) isomers without the hydroxyl as a H-bond donor to a water molecule (green \bullet); (d) isomers with the "AA" motif (orange \bullet) and isomers without the hydroxyl hydrogen atom as a H-bond donor to a water molecule (green \circ).

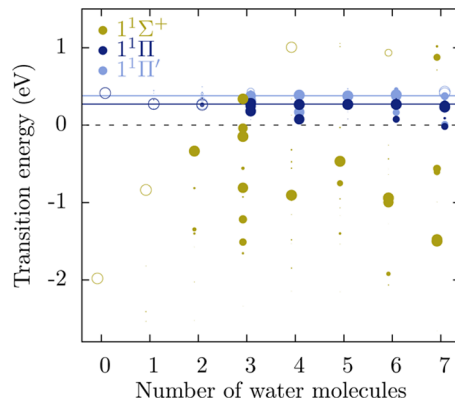


Figure 8. Transition energies from the $1^3\Pi$ state to the three lowest singlet states ($1^1\Sigma^+$, $1^1\Pi$, and $1^1\Pi'$) of $\text{OH}^-(\text{H}_2\text{O})_n$ clusters, at geometries optimized in the $1^3\Pi$ state (cf. Figure 5). Results are calculated at the RASPT2/aug-cc-pVTZ level. Dark and light blue lines correspond to the mean transition energy from the $1^3\Pi$ state to the $1^1\Pi$ and $1^1\Pi'$ states, respectively, over all sizes and isomers. For the symbol legend, see Figure 3.

a broad distribution of VDEs around this linear increase. To shed light on the physical properties responsible for this broad distribution, we plot in Figure 7c,d the VDEs of the $1^3\Pi$ state for $1^3\Pi$ structures as a function of selected clustering patterns, given at the end of section 4.1. For the sake of clarity, only the $1^3\Pi$ state is represented, but the following considerations also stand for the other Π states. Black hollow circles display all isomers, without any selection.

In Figure 7c, green solid circles show the isomers for which the hydroxyl hydrogen atom does not donate a H bond to water molecules, as given in Table 2. These isomers display VDE values which are located at the top of the distribution, due to a strongly perturbed $1^2\Pi$ state of the corresponding neutral species. In these isomers (cf. isomers 3k, 3l, and 3m of Figure 5, for example), the excess electron is “solvated” within a cage of dangling Hs that belong to both the hydroxyl radical and water molecules. Therefore, when this electron is removed to obtain the neutral species, the dangling Hs face each other. As they

present a partial positive charge, electrostatic interaction makes them repel each other and provokes an increase of the $1^2\Pi$ state energy, along with a corresponding increase of the VDEs.

The rest of the isomers, which present the OH hydrogen as a H-bond donor, have lower VDEs. Their dangling Hs and their excess electron are located at the surface, and the hydroxyl radical belongs to the H-bond network. As a result, the electrostatic repulsion between the dangling Hs for the neutral system remains smaller than that for the previous set of isomers.

Isomers containing the “AA” motif, displayed with orange solid circles in Figure 7d, show enhanced VDEs. Not surprisingly, “AA” isomers provide greater VDEs in comparison to isomers with single acceptor motifs, as the “AA” motif not only enables a better stabilization of the excess electron but also displays an enhanced repulsion between dangling Hs in the neutral system. This enhanced repulsion is due to a shorter distance between hydrogen atoms that belong to the same water molecule rather than to different ones. Therefore, both effects of the “AA” motif are in favor of large VDEs, by lowering the anionic Π states and increasing the neutral $1^2\Pi$ state.

4.3. Transition Energies.

Transition energies from the $1^3\Pi$ state to the singlet states, $1^1\Sigma^+$, $1^1\Pi$, and $1^1\Pi'$, at $1^3\Pi$ equilibrium geometries, are plotted in Figure 8.

The $1^1\Pi$ and $1^1\Pi'$ states, displayed by dark and light blue points, respectively, show quasi-constant transition energies for all isomers, whatever the size or structure, as for the $1^1\Sigma^+$ relaxed structures. Small deviations occur around the mean transition energies over all isomers and sizes, represented with dark and light blue lines for $1^1\Pi$ and $1^1\Pi'$ states, respectively. For small clusters, some isomers have a symmetry that lifts the degeneracy of Π states, in contrast to the case for unsymmetrical larger clusters. For some isomers of the larger clusters, the $1^3\Pi$ and $1^1\Pi$ states get closer in energy; in some cases, the expected energy ordering is even inverted. This indicates that a coupling exists among all singlet states at these geometries, and in particular with the $1^1\Sigma^+$ ground state. However, these deviations concern a limited number of isomers and remain in all cases smaller than 0.25 eV.

The transition energies from the $1^3\Pi$ state to the $1^1\Sigma^+$ state is far more complicated, as it implies two states of very different

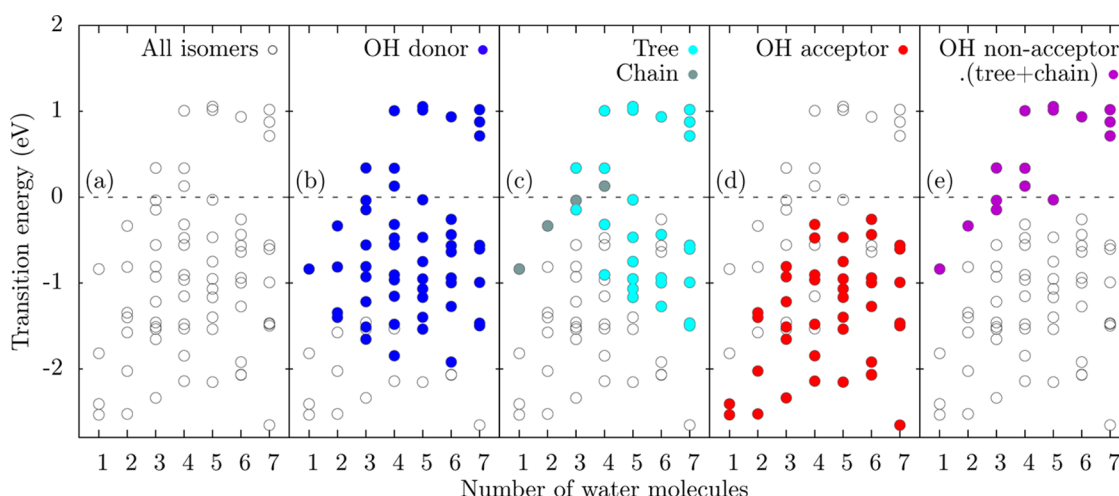


Figure 9. Transition energies from the $1^3\Pi$ state to the $1^1\Sigma^+$ state of $\text{OH}^-(\text{H}_2\text{O})_n$ clusters, at geometries optimized in the $1^3\Pi$ state (cf. Figure 5). The results are calculated at the RASPT2/aug-cc-pVTZ level. Open circles display all isomers, and solid circles display the isomers fulfilling the selected criterion: (a) all isomers; (b) isomers with the hydroxyl hydrogen atom as a H-bond donor to a water molecule (dark blue ●); (c) isomers with the tree pattern (light blue ●) or chain pattern (gray ●); (d) isomers with the hydroxyl oxygen atom as a H-bond acceptor from a water molecule (red ●); (e) isomers with the tree pattern or chain pattern and without the hydroxyl oxygen atom as a H-bond acceptor from a water molecule (purple ●).

chemical nature, reflected by a broad energy distribution. In comparison to $1^1\Sigma^+$ relaxed structures (cf. Figure 4), these transition energies are smaller and grow in opposite ways with the number of water molecules. A very interesting feature of the distribution is the inversion of the Π and the $1^1\Sigma^+$ states for several isomers: i.e., with a positive transition energy. This inversion indicates the existence of an avoided crossing in the vicinity of the local or sometimes global minima, which might participate in the recombination of $\text{OH}^-(\text{H}_2\text{O})_n$ clusters following an excitation in one of their CTTS states.

To analyze the broad distribution of transition energies from the $1^3\Pi$ to the $1^1\Sigma^+$ state, we report in Figure 9 these energies as a function of structural considerations. Figure 9a displays these transition energies for all isomers, without any selection, represented by open circles. In Figure 9b, we first compare the isomers providing (blue ●) or not providing (○) the donation of a H bond from a hydroxyl hydrogen to a water molecule. Clearly, isomers that display the OH as a donor appear to have larger values, by about 1 eV above other isomers, in agreement with the observations made for the “solvated” isomer in section 3.2. This donation belongs to the optimum clustering pattern. Therefore, it stabilizes and lowers the $1^3\Pi$ state energy. At the same time, this donation strongly perturbs the $1^1\Sigma^+$ state, as the water molecule stands in a repulsive part of the $1^1\Sigma^+$ PES.

This increase of the $1^1\Sigma^+$ state energy with respect to the $1^3\Pi$ state energy is even enhanced by adding more water molecules to the hydrogen side of OH. This effect is highlighted in Figure 9c by selecting the $1^3\Pi$ structures containing the tree (light blue ●) or the chain (gray ●) pattern, which necessarily have the OH as a donor.

The lower part of the transition energy distribution is explained by the presence of one or even two water molecules that donate a H bond to the hydroxyl, i.e. with the OH as an acceptor, as depicted by red ● symbols in Figure 9d. Such a positioning of the water molecules has only a slight effect on Π states but is substantial on the lowering of the $1^1\Sigma^+$ state, where the excess electron is well-localized on the OH oxygen atom.

Finally, we selected in Figure 9e by purple ● symbols the isomers that display the tree or chain pattern and that do not present the OH in a position of a H-bond acceptor. We found that these isomers provide the very top of the transition energy distribution and are the only isomers that enable the inversion of the $1^1\Sigma^+$ and $1^3\Pi$ states (i.e. with a positive transition energy) for these small cluster sizes. However, as the transition energies globally increase with the number of water molecules, the considered selection criteria for these isomers are not necessarily mandatory to obtain the inversion for larger clusters or in solution.

5. CONCLUSION AND PERSPECTIVES

We investigated the ground and lowest excited states of $\text{OH}^-(\text{H}_2\text{O})_n$ clusters by means of the RASPT2 method.

For $1^1\Sigma^+$ ground state structures, water molecule positioning occurs first by the donation of up to three or four H bonds to the hydroxide oxygen atom, which mainly carries the excess charge. The $\text{OH}^-/\text{H}_2\text{O}$ bonding is the dominant molecular interaction, due mainly to the strong polarization of water molecules induced by the hydroxide, along with partial covalence and charge transfer from the hydroxide to the first water solvation shell. Then, from these three- or four-bond patterns, water molecules organize themselves to optimize the H-bond network of water, i.e. to maximize coordination, leaving in any case the hydroxide at the surface. For each size, the lowest energy structures are in good

agreement with previous studies,^{23,60} with some deviation regarding the details of bond lengths and angles.

We established that, by increasing the number of water molecules, a strong stabilization of the hydroxide occurs, along with an increase of VDEs and transition energies from $1^1\Sigma^+$ to excited states, both converging to the experimental bulk values. These observables have been found to be nearly insensitive to structural properties, although they are very size sensitive. Then, we evaluated the influence of a weak H bond between water oxygen and hydroxide hydrogen, evidenced experimentally in the aqueous phase,⁵³ and we revealed that it significantly increases the energy of the $1^1\Sigma^+$ state, while leaving Π states unchanged. These Π states, which are not bound in the free OH^- , start to be bound for $n = 1$ and $n = 3$ for the $1^3\Pi$ state and $1^3\Pi'$, $1^1\Pi$, and $1^1\Pi'$ states, respectively.

Our pioneering study of geometries optimized in the $1^3\Pi$ excited state provides new insights at the atomic level on the so-called “contact pair” $\text{OH}:e^-$ following CTTS excitation in the aqueous phase.¹⁶ From the numerous isomers optimized, it emerges that the structures in the excited state strongly differ from $1^1\Sigma^+$ ground state structures. The excess electron is preferentially stabilized on water molecules rather than on the hydroxide. Minimum energy structures are characterized by the hydroxide as a H-bond donor, over which tree and chain motifs grow. These key motifs enable the excess electron transfer from the hydroxide to the dangling Hs of water molecules, to eventually form an almost neutral hydroxyl radical in a water network. Then, from the tree motif, water molecules cluster to form $2n - 2$ H bonds, which is the maximum number of bonds that can be formed without strong structural constraints. It thus leaves three dangling Hs, and among them, the double-acceptor motif shows an enhanced stabilization of the excess electron in comparison to single-acceptor motifs. However, this “AA” motif cannot be formed for a few specific cluster sizes because of limitations in geometric arrangements.

Concerning the VDEs, we found that the $1^3\Pi$ state values are size sensitive due to the excess charge-induced polarization that increases with cluster size. They are, however, nearly insensitive to the different structural conformations, because of the strong chemical and structural similarities of the Π states with the ground state of the neutral system. In contrast, the $1^1\Sigma^+$ state at $1^3\Pi$ geometries displays a strong sensitivity to clustering patterns. Its energy increases when water molecules are H-bond acceptors from the OH hydrogen, as for tree or chain motifs, while it decreases when they are H-bond donors to the OH oxygen, as for $1^1\Sigma^+$ structures. Furthermore, some of the most stable $1^3\Pi$ structures exhibit a $1^1\Sigma^+$ state higher in energy than Π states, sign of a strong coupling between ground and excited states. Such geometries are likely to play a significant role for recombination in solution.

In view of our new insights into the initial excitation in the CTTS state and the final clustering patterns driven by the CTTS state relaxation, we propose a possible scenario for the geminate recombination of OH and the excess electron after a CTTS state excitation in the aqueous phase. Initially, the hydroxide in its ground state is solvated, accepting almost four strong H bonds at its oxygen side and donating a weak bond from its hydrogen side. From this configuration, excitation in the CTTS state occurs, initiating the relaxation. The charge initially localized on the hydroxide oxygen goes to the hydroxide hydrogen side. As a result, the weak bond donated by the hydroxide shortens to form a strong one, as observed in our $1^3\Pi$ structures, which enables the transfer of the excess charge to the corresponding acceptor water molecule

area, and then the presolvation of the excited state. The hydroxyl radical, left behind, is a weak hydrogen acceptor, accepting only one or two water molecules,⁶¹ with longer equilibrium distances than OH⁻ in its ground state. Therefore, the hydroxyl is repelled by the four donor water molecules, provoking its migration in the direction of its hydrogen in the initial solvation cage, combined with the loss of H bonds. This molecular reorganization induces a strong increase of the 1¹ Σ^+ state energy. The 1¹ Σ^+ state can then get close enough to the CTTS states to enable nonradiative transition back to the 1¹ Σ^+ state. Once in the 1¹ Σ^+ state, the system relaxes, giving its excess vibrational energy to the solvent, to eventually build new bonds and re-form the initial OH⁻ molecule.

Of course, the extrapolation from our static pictures of the CTTS state to its dynamics, as well as the extrapolation from small clusters to the bulk phase, should be investigated by means of molecular dynamics simulations to get firmer ground. In any case, our study supports that such a straightforward scenario is likely to occur in aqueous solutions.

ASSOCIATED CONTENT

Supporting Information

xyz files giving Cartesian coordinates of OH⁻(H₂O)_n clusters optimized in the 1¹ Σ^+ and 1³ Π states with the RASPT2 method, shown in Figures 1 and 5, respectively. The Supporting Information is available free of charge on the ACS Publications website at DOI: 10.1021/acs.jpca.5b03893.

AUTHOR INFORMATION

Corresponding Authors

*D.Z.: e-mail, zanuttini@ganil.fr.

*B.G.: tel, +33 (0)2 31 45 47 93; fax, +33 (0)2 31 45 47 14; e-mail, gervais@ganil.fr.

Notes

The authors declare no competing financial interest.

ACKNOWLEDGMENTS

This work was supported by INSERM through Plan Cancer Program 2009–2013 (NANOBIODOS project) and the Région Basse-Normandie.

REFERENCES

- Petersen, C.; Thøgersen, J.; Jensen, S. K.; Keiding, S. R. Electron Detachment and Relaxation of OH⁻(aq). *J. Phys. Chem. A* **2007**, *111*, 11410–11420.
- Young, R. M.; Neumark, D. M. Dynamics of Solvated Electrons in Clusters. *Chem. Rev.* **2012**, *112*, 5553–5577.
- Migus, A.; Gauduel, Y.; Martin, J. L.; Antonetti, A. Excess Electrons in Liquid Water: First Evidence of a Prehydrated State with Femtosecond Lifetime. *Phys. Rev. Lett.* **1987**, *58*, 1559–1562.
- Laenen, R.; Roth, T.; Laubereau, A. Novel Precursors of Solvated Electrons in Water: Evidence for a Charge Transfer Process. *Phys. Rev. Lett.* **2000**, *85*, 50–53.
- Newton, M. D. Role of *Ab Initio* Calculations in Elucidating Properties of Hydrated and Ammoniated Electrons. *J. Phys. Chem.* **1975**, *79*, 2795–2808.
- Turi, L.; Borgis, D. Analytical Investigations of an Electron-water Molecule Pseudopotential. II. Development of a New Pair Potential and Molecular Dynamics Simulations. *J. Chem. Phys.* **2002**, *117*, 6186–6195.
- Schnitker, J.; Rossky, P. J. Quantum Simulation Study of the Hydrated Electron. *J. Chem. Phys.* **1987**, *86*, 3471–3485.
- Herbert, J. M.; Jacobson, L. D. Structure of the Aqueous Electron: Assessment of One-Electron Pseudopotential Models in Comparison to Experimental Data and Time-Dependent Density Functional Theory. *J. Phys. Chem. A* **2011**, *115*, 14470–14483.
- Turi, L.; Rossky, P. J. Theoretical Studies of Spectroscopy and Dynamics of Hydrated Electrons. *Chem. Rev.* **2012**, *112*, 5641–5674.
- Larsen, R. E.; Glover, W. J.; Schwartz, B. J. Does the Hydrated Electron Occupy a Cavity? *Science* **2010**, *329*, 65–69.
- Bradforth, S. E.; Jungwirth, P. Excited States of Iodide Anions in Water: A Comparison of the Electronic Structure in Clusters and in Bulk Solution. *J. Phys. Chem. A* **2002**, *106*, 1286–1298.
- Elola, M. D.; Laria, D. Solvation Dynamics Following Electron Photodetachment from I⁻ in Aqueous Clusters. *J. Chem. Phys.* **2002**, *117*, 2238–2245.
- Kolaski, M.; Lee, H. M.; Pak, C.; Dupuis, M.; Kim, K. S. *Ab Initio* Molecular Dynamics Simulations of an Excited State of X⁻(H₂O)₃ (X = Cl, I) Complex. *J. Phys. Chem. A* **2005**, *109*, 9419–9423.
- Sheu, W.-S.; Rossky, P. J. Electronic and Solvent Relaxation Dynamics of a Photoexcited Aqueous Halide. *J. Phys. Chem.* **1996**, *100*, 1295–1302.
- Igley, H.; Fischer, M. K.; Laubereau, A. Electron Detachment from Anions in Aqueous Solutions Studied by Two- and Three-Pulse Femtosecond Spectroscopy. *Pure Appl. Chem.* **2010**, *82*, 1919–1926.
- Igley, H.; Fischer, M. K.; Gliserin, A.; Laubereau, A. Ultrafast Geminate Recombination after Photodetachment of Aqueous Hydroxide. *J. Am. Chem. Soc.* **2011**, *133*, 790–795.
- Garrett, B. C.; Dixon, D. A.; Camaiori, D. M.; Chipman, D. M.; Johnson, M. A.; Jonah, C. D.; Kimmel, G. A.; Miller, J. H.; Rescigno, T. N.; Rossky, P. J.; et al. Role of Water in Electron-Initiated Processes and Radical Chemistry: Issues and Scientific Advances. *Chem. Rev.* **2005**, *105*, 355–390.
- Nguyen, J.; Ma, Y.; Luo, T.; Bristow, R. G.; Jaffray, D. A.; Lu, Q.-B. Direct Observation of Ultrafast-Electron-Transfer Reactions Unravels High Effectiveness of Reductive DNA Damage. *Proc. Natl. Acad. Sci. U. S. A.* **2011**, *108*, 11778–11783.
- Kohn, W. Nobel Lecture: Electronic Structure of Matter—Wave Functions and Density Functionals. *Rev. Mod. Phys.* **1999**, *71*, 1253–1266.
- Møller, C.; Plesset, M. S. Note on an Approximation Treatment for Many-Electron Systems. *Phys. Rev.* **1934**, *46*, 618–622.
- Warshel, A.; Weiss, R. M. An Empirical Valence Bond Approach for Comparing Reactions in Solutions and in Enzymes. *J. Am. Chem. Soc.* **1980**, *102*, 6218–6226.
- Chaudhuri, C.; Wang, Y.-S.; Jiang, J. C.; Lee, Y. T.; Chang, H.-C.; Niedner-Schattburg, G. Infrared Spectra and Isomeric Structures of Hydroxide Ion-Water Clusters OH⁻(H₂O)_{1–5}: a Comparison with H₃O⁺(H₂O)_{1–5}. *Mol. Phys.* **2001**, *99*, 1161–1173.
- Bryantsev, V. S.; Diallo, M. S.; van Duin, A. C. T.; Goddard, W. A., III Evaluation of B3LYP, X3LYP, and M06-Class Density Functionals for Predicting the Binding Energies of Neutral, Protonated, and Deprotonated Water Clusters. *J. Chem. Theory Comput.* **2009**, *5*, 1016–1026.
- Bankura, A.; Chandra, A. Hydration Structure and Dynamics of a Hydroxide Ion in Water Clusters of Varying Size and Temperature: Quantum Chemical and *Ab Initio* Molecular Dynamics Studies. *Chem. Phys.* **2012**, *400*, 154–164.
- Ufimtsev, I. S.; Kalinichev, A. G.; Martinez, T. J.; James Kirkpatrick, R. A Multistate Empirical Valence Bond Model for Solvation and Transport Simulations of OH⁻ in Aqueous Solutions. *Phys. Chem. Chem. Phys.* **2009**, *11*, 9420–9430.
- Tuckerman, M. E.; Marx, D.; Parrinello, M. The Nature and Transport Mechanism of Hydrated Hydroxide Ions in Aqueous Solution. *Nature* **2002**, *417*, 925–929.
- Malmqvist, P. Å.; Pierloot, K.; Shahi, A. R. M.; Cramer, C. J.; Gagliardi, L. The Restricted Active Space Followed by Second-Order Perturbation Theory Method: Theory and Application to the Study of CuO₂ and Cu₂O₂ Systems. *J. Chem. Phys.* **2008**, *128*, 204109.
- Andersson, K.; Malmqvist, P.-Å.; Roos, B. O.; Sadlej, A. J.; Wolinski, K. Second-Order Perturbation Theory with a CASSCF Reference Function. *J. Phys. Chem.* **1990**, *94*, 5483–5488.

- (29) Andersson, K.; Malmqvist, P.-Å.; Roos, B. O. Second-Order Perturbation Theory with a Complete Active Space Self-Consistent Field Reference Function. *J. Chem. Phys.* **1992**, *96*, 1218–1226.
- (30) Finley, J.; Malmqvist, P.-Å.; Roos, B. O.; Serrano-Andrés, L. The Multi-State CASPT2 Method. *Chem. Phys. Lett.* **1998**, *288*, 299–306.
- (31) Roos, B. O.; Taylor, P. R.; Siegbahn, P. E. M. A Complete Active Space SCF Method (CASSCF) Using a Density Matrix Formulated Super-CI Approach. *Chem. Phys.* **1980**, *48*, 157–173.
- (32) Gdanitz, R. J.; Ahlrichs, R. The Averaged Coupled-Pair Functional (ACPF): A Size-Extensive Modification of MR CI(SD). *Chem. Phys. Lett.* **1988**, *143*, 413–420.
- (33) Masamura, M. Structures, Energetics, and Spectra of OH⁻(H₂O)_n and SH⁻(H₂O)_n Clusters, n=1–5: *Ab Initio* study. *J. Chem. Phys.* **2002**, *117*, 5257–5263.
- (34) Dunning, T. H. Gaussian Basis Sets for Use in Correlated Molecular Calculations. I. The Atoms Boron Through Neon and Hydrogen. *J. Chem. Phys.* **1989**, *90*, 1007–1023.
- (35) Kendall, R. A.; Dunning, T. H.; Harrison, R. J. Electron Affinities of the First-Row Atoms Revisited. Systematic Basis Sets and Wave Functions. *J. Chem. Phys.* **1992**, *96*, 6796–6806.
- (36) Boys, S.; Bernardi, F. The Calculation of small Molecular Interactions by the Differences of Separate Total Energies. Some Procedures With Reduced Errors. *Mol. Phys.* **1970**, *19*, 553–566.
- (37) Salvador, P.; Duran, M.; Dannenberg, J. J. Counterpoise Corrected Ion/Molecule Complexes Using Two or Three Fragments. *J. Phys. Chem. A* **2002**, *106*, 6883–6889.
- (38) Mentel, Å. M.; Baerends, E. J. Can the Counterpoise Correction for Basis Set Superposition Effect Be Justified? *J. Chem. Theory Comput.* **2014**, *10*, 252–267.
- (39) Gagliardi, L.; Lindh, R.; Karlström, G. Local Properties of Quantum Chemical Systems: The LoProp Approach. *J. Chem. Phys.* **2004**, *121*, 4494–4500.
- (40) Mulliken, R. S. Criteria for the Construction of Good Self-Consistent-Field Molecular Orbital Wave Functions, and the Significance of LCAO-MO Population Analysis. *J. Chem. Phys.* **1962**, *36*, 3428–3439.
- (41) Löwdin, P.-O. On the Nonorthogonality Problem. *Adv. Quantum Chem.* **1970**, *5*, 185–199.
- (42) Reed, A. E.; Curtiss, L. A.; Weinhold, F. Intermolecular Interactions from a Natural Bond Orbital, Donor-Acceptor Viewpoint. *Chem. Rev.* **1988**, *88*, 899–926.
- (43) Aquilante, F.; De Vico, L.; Ferré, N.; Ghigo, G.; Malmqvist, P.-Å.; Neogrády, P.; Pedersen, T. B.; Pitoňák, M.; Reiher, M.; Roos, B. O.; et al. MOLCAS 7: The Next Generation. *J. Comput. Chem.* **2010**, *31*, 224–247.
- (44) Schaftenaar, G.; Noordik, J. Molden: a Pre- and Post-Processing Program for Molecular and Electronic Structures. *J. Comput.-Aided Mol. Des.* **2000**, *14*, 123–134.
- (45) Wales, D. J.; Doye, J. P. K.; Dullweber, A.; Hodges, M. P.; Naumkin, F. Y.; Calvo, F.; Hernández-Rojas, J.; Middleton, T. F. The Cambridge Cluster Database. <http://www-wales.ch.cam.ac.uk/CCD.html>, date of access: 2015-03-30.
- (46) Maheshwary, S.; Patel, N.; Sathyamurthy, N.; Kulkarni, A. D.; Gadre, S. R. Structure and Stability of Water Clusters (H₂O)_n, n = 8–20: An *Ab Initio* Investigation. *J. Phys. Chem. A* **2001**, *105*, 10525–10537.
- (47) Botti, A.; Bruni, F.; Imberti, S.; Ricci, M.; Soper, A. Solvation Shell of OH⁻ Ions in Water. *J. Mol. Liq.* **2005**, *117*, 81–84.
- (48) Ma, Z.; Tuckerman, M. E. On the Connection Between Proton Transport, Structural Diffusion, and Reorientation of the Hydrated Hydroxide Ion as a Function of Temperature. *Chem. Phys. Lett.* **2011**, *511*, 177–182.
- (49) Crawford, T. D.; Schaefer, H. F.; Lee, T. J. On the Energy Invariance of Open-Shell Perturbation Theory with Respect to Unitary Transformations of Molecular Orbitals. *J. Chem. Phys.* **1996**, *105*, 1060–1069.
- (50) Sakai, K.; Watanabe, I.; Yokoyama, Y. Vertical Ionization Potentials of Alkoxides in Solution. *Bull. Chem. Soc. Jpn.* **1994**, *67*, 360–362.
- (51) Winter, B.; Faubel, M.; Hertel, I. V.; Pettenkofer, C.; Bradford, S. E.; Jagoda-Cwiklik, B.; Cwiklik, L.; Jungwirth, P. Electron Binding Energies of Hydrated H₃O⁺ and OH⁻: Photoelectron Spectroscopy of Aqueous Acid and Base Solutions Combined with Electronic Structure Calculations. *J. Am. Chem. Soc.* **2006**, *128*, 3864–3865.
- (52) von Burg, K.; Delahay, P. Photoelectron Emission Spectroscopy of Inorganic Anions in Aqueous Solution. *Chem. Phys. Lett.* **1981**, *78*, 287–290.
- (53) Megyes, T.; Bálint, S.; Grósz, T.; Radnai, T.; Bakó, I.; Sipos, P. The Structure of Aqueous Sodium Hydroxide Solutions: A Combined Solution X-Ray Diffraction and Simulation Study. *J. Chem. Phys.* **2008**, *128*, 044501.
- (54) Marx, D.; Chandra, A.; Tuckerman, M. E. Aqueous Basic Solutions: Hydroxide Solvation, Structural Diffusion, and Comparison to the Hydrated Proton. *Chem. Rev.* **2010**, *110*, 2174–2216.
- (55) Blandamer, M. J.; Fox, M. F. Theory and Applications of Charge-Transfer-To-Solvent Spectra. *Chem. Rev.* **1970**, *70*, 59–93.
- (56) Fox, M.; McIntyre, R.; Hayon, E. Far Ultraviolet Solution Spectroscopy of Hydroxide. *Faraday Discuss. Chem. Soc.* **1977**, *64*, 167–172.
- (57) Herbert, J. M.; Head-Gordon, M. Accuracy and Limitations of Second-Order Many-Body Perturbation Theory for Predicting Vertical Detachment Energies of Solvated-Electron Clusters. *Phys. Chem. Chem. Phys.* **2006**, *8*, 68–78.
- (58) Hammer, N. I.; Roscioli, J. R.; Johnson, M. A. Identification of Two Distinct Electron Binding Motifs in the Anionic Water Clusters: A Vibrational Spectroscopic Study of the (H₂O)_n⁻ Isomers. *J. Phys. Chem. A* **2005**, *109*, 7896–7901.
- (59) Hammer, N. I.; Roscioli, J. R.; Johnson, M. A.; Myshakin, E. M.; Jordan, K. D. Infrared Spectrum and Structural Assignment of the Water Trimer Anion. *J. Phys. Chem. A* **2005**, *109*, 11526–11530.
- (60) Robertson, W. H.; Diken, E. G.; Price, E. A.; Shin, J.-W.; Johnson, M. A. Spectroscopic Determination of the OH⁻ Solvation Shell in the OH⁻(H₂O)_n Clusters. *Science* **2003**, *299*, 1367–1372.
- (61) Galbis, E.; Giglio, E.; Gervais, B. A Diabatic Parameterization of the Twofold Ground State Potential Energy Surface of the H₂O-OH Molecular Complex. *J. Chem. Phys.* **2013**, *139*, 164313.